CHEMISTRY OF MATERIALS
Article

Chem. Mater. **2010,** *22,* 2033–2040 2033
DOI:10.1021/cm100124a

Atomic-Scale Investigation of Two-Component MoVO Complex Oxide Catalysts Using Aberration-Corrected High-Angle Annular Dark-Field Imaging

William D. Pyrz,[†] Douglas A. Blom,[‡] Masahiro Sadakane,[§] Katsunori Kodato,[⊥] Wataru Ueda,[⊥] Thomas Vogt,[#] and Douglas J. Buttrey*,[†]

[†]*Center for Catalytic Science and Technology, Department of Chemical Engineering, University of Delaware, Newark, Delaware 19716,* [‡]*NanoCenter and Electron Microscopy Center, and* [#]*NanoCenter and Department of Chemistry and Biochemistry, University of South Carolina, Columbia, South Carolina 29208, and* [⊥]*Catalysis Research Center, Hokkaido University, N-21, W-10, Sapporo, 001-0021 (Japan).* [§]*Current address: Chemistry and Chemical Engineering, Department of Engineering, Hiroshima University, 1-4-1 Kagamiyama, Higashi-Hiroshima, 739-8527, Japan.*

Received January 14, 2010

High-angle annular dark-field (HAADF) scanning transmission electron microscopy (STEM) imaging was used to study various hydrothermally prepared MoVO phases with either M1-type orthorhombic symmetry, Mo_5O_{14}-type tetragonal symmetry, or trigonal symmetry. For the M1-type phase, HAADF analysis suggests atomic positions consistent with existing M1 models having mixed Mo and V occupancy in the octahedral sites linking the pentagonal units. For the V-substituted Mo_5O_{14} phase, contrast analysis provides evidence of V occupation primarily in the linking octahedra that interconnect the pentagonal $\{Mo_6O_{21}\}$ units. Selected-area electron diffraction (SAED) studies suggest that the structure of the Mo_5O_{14} analog is likely to be tetragonal, rather than orthorhombically distorted as has previously been proposed. HAADF analysis of the trigonal phase provides reasonable support for previously reported structural models. High-resolution images provide strong support for the existence of atomic disorder within the octahedral sites connecting the three heptagonal channels that characterize this structure.

1. Introduction

Molybdenum-based suboxides have been a subject of extensive research for several decades. One class consists of bronzes based on pentagonal $\{Mo_6O_{21}\}$ building units; these include Mo_5O_{14} and $Mo_{17}O_{47}$.[1−6] In the last 20 years, new materials doped with a variety of substitution elements, but built upon the same structural building units, have attracted significant interest for catalytic applications. These applications include the selective oxidation of light paraffins and olefins, as well as the partial oxidation of methanol.[7−18] Depending on the species substituted and the combination of phases present, catalytic performance seems to vary significantly.[18−21] Example systems include MoVNbTeO,[22−26]

*Corresponding author. E-mail: dbuttrey@udel.edu. Phone: (302) 831-2034. Fax: (302) 831-2085.

(1) Kihlborg, L. *Arkiv Kemi* **1964**, *21*, 471.
(2) Yamazoe, N.; Ekstrom, T.; Kihlborg, L. *Acta Chem. Scand. A: Phys. Inorg. Chem.* **1975**, *29*, 404.
(3) Yamazoe, N.; Kihlborg, L. *Acta Crystallogr., Sect. B* **1975**, *31*, 1666.
(4) Ekstrom, T. *Mater. Res. Bull.* **1972**, *7*, 19.
(5) Ekstrom, T.; Iguchi, E.; Tilley, R. J. D. *Acta Chem. Scand. A: Phys. Inorg. Chem.* **1976**, *30*, 312.
(6) Ekstrom, T.; Nygren, M. *Acta Chem. Scand.* **1972**, *26*, 1827.
(7) Baca, M.; Pigamo, A.; Dubois, J. L.; Millet, J. M. M. *Top. Catal.* **2003**, *23*, 39.
(8) Grasselli, R. K. *Top. Catal.* **2002**, *21*, 79.
(9) Grasselli, R. K. *Catal. Today* **2005**, *99*, 23.
(10) Mestl, G. *Top. Catal.* **2006**, *38*, 69.
(11) Mestl, G.; Linsmeier, C.; Gottschall, R.; Dieterle, M.; Find, J.; Herein, D.; Jager, J.; Uchida, Y.; Schlogl, R. *J. Mol. Catal. A: Chem.* **2000**, *162*, 455.
(12) López Nieto, J. M.; Botella, P.; Vázquez, M. I.; Dejoz, A. *Chem. Commun.* **2002**, 1906.
(13) Shiju, N. R.; Liang, X. H.; Weimer, A. W.; Liang, C.; Dai, S.; Guliants, V. V. *J. Am. Chem. Soc.* **2008**, *130*, 5850.
(14) Ueda, W.; Vitry, D.; Kato, T.; Watanabe, N.; Endo, Y. *Res. Chem. Intermed.* **2006**, *32*, 217.
(15) Ushikubo, T.; Oshima, K.; Kayou, A.; Vaarkamp, M.; Hatano, M. *J. Catal.* **1997**, *169*, 394.
(16) Vitry, D.; Morikawa, Y.; Dubois, J. L.; Ueda, W. *Appl. Catal., A* **2003**, *251*, 411.
(17) Wagner, J. B.; Timpe, O.; Hamid, F. A.; Trunschke, A.; Wild, U.; Su, D. S.; Widi, R. K.; Abd Hamid, S. B.; Schlogl, R. *Top. Catal.* **2006**, *38*, 51.
(18) Watanabe, N.; Ueda, W. *Ind. Eng. Chem. Res.* **2006**, *45*, 607.
(19) Grasselli, R. K.; Buttrey, D. J.; Burrington, J. D.; Andersson, A.; Holmberg, J.; Ueda, W.; Kubo, J.; Lugmair, C. G.; Volpe, A. F. *Top. Catal.* **2006**, *38*, 7.
(20) Holmberg, J.; Grasselli, R. K.; Andersson, A. *Top. Catal.* **2003**, *23*, 55.
(21) Holmberg, J.; Grasselli, R. K.; Andersson, A. *Appl. Catal., A* **2004**, *270*, 121.
(22) Botella, P.; López Nieto, J. M.; Solsona, B.; Mifsud, A.; Marquez, F. *J. Catal.* **2002**, *209*, 445.
(23) (a) Grasselli, R. K.; Buttrey, D. J.; DeSanto, P.; Burrington, J. D.; Lugmair, C. G.; Volpe, A. F.; Weingand, T. *Catal. Today* **2004**, *91−92*, 251. (b) Grasselli, R. K.; Burrington, J. D.; Buttrey, D. J.; DeSanto, P.; Lugmair, C. G.; Volpe, A. F.; Weingand, T. *Top. Catal.* **2003**, *23*, 5.
(24) Oliver, J. M.; López Nieto, J. M.; Botella, P. *Catal. Today* **2004**, *96*, 241.
(25) Pyrz, W. D.; Blom, D. A.; Vogt, T.; Buttrey, D. J. *Angew. Chem., Int. Ed.* **2008**, *47*, 2788.
(26) Sanfiz, A. C.; Hansen, T. W.; Girgsdies, F.; Timpe, O.; Rodel, E.; Ressler, T.; Trunschke, A.; Schlogl, R. *Top. Catal.* **2008**, *50*, 19.

© 2010 American Chemical Society
Published on Web 02/03/2010

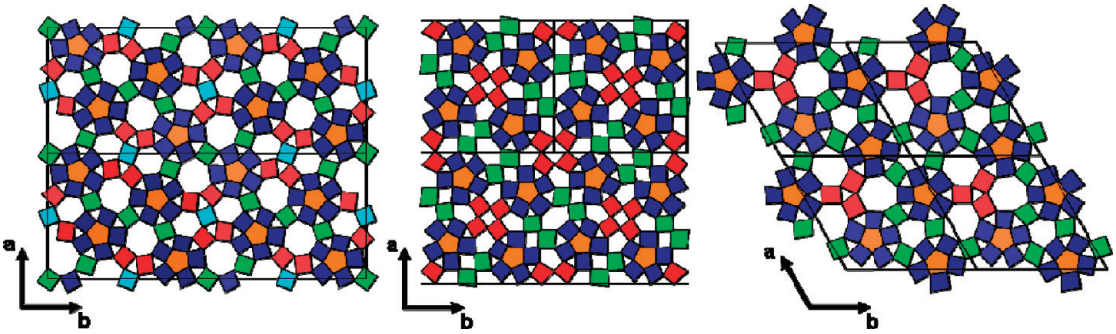

Figure 1. Ideal two-dimensional 2 × 2 unit cells for three MoVO structures: M1-type (left), Mo_5O_{14}-type (center), and trigonal (right). The $Mo_{17}O_{47}$ framework is not shown because it seems not to exist with significant vanadium substitution.

MoVTaTeO,[19,27,28] MoVTeO,[29,30] MoVO,[14,31,32] MoVWO,[10,11,33,34] and MoVSbO.[35−37]

To explain the catalytic differences observed in these systems, recent reports have proposed two distinct mechanisms. One mechanism originally proposed by Grasselli et al. for the Mo−V−Nb−Te−O mixed metal oxide system suggests that the catalysis occurs on well-ordered and isolated active sites that are found on the (001) crystalline face.[9,19,23] The second mechanism, proposed by Wagner et al., suggests that the catalysis does not require well-ordered and isolated active sites, but can also occur on any crystalline face, ordered or disordered, provided that the appropriate active components are present on the surface.[17] In either case, we believe that a thorough understanding of the crystalline framework is critical, because it is likely that the underlying bulk material will influence the organization and composition of the catalyst surface. We believe that this will be the case regardless of whether or not the crystalline faces terminate with an ordered arrangement matching that of the bulk framework or if termination involves a slightly disordered structure. Therefore, there is interest in isolating and characterizing the individual phases present in these mixed-metal oxides systems in order to develop and improve our understanding of composition−structure−performance relationships.

At least four different structural frameworks derived from pentagonal $\{Mo_6O_{21}\}$ building units are known; these are the orthorhombic (M1-type),[38,39] pseudotetragonal (Mo_5O_{14}-type),[1,3] the $Mo_{17}O_{47}$-type,[40] and the most recently discovered trigonal phase[31] (Figure 1). An additional closely related framework with pentagonal units of this type also exists in the tungsten family with composition $W_{18}O_{49}$.[41] We are not aware of the existence of a molybdenum analog to this latter framework. The orthorhombic (M1-type) structure was initially observed in the Cs−Nb−W-O system studied by Lundberg and Sundberg.[42] About a decade later, this structure-type has been identified in the Mo−V−O-based complex oxide catalysts and has been synthesized using MoVO,[14,31,32] MoVTeO,[29,30] MoVNbTeO,[22−26] MoVTaTeO,[19,27,28] and MoVSbO[35−37] formulations. The unit cell for this structure contains four $\{Mo_6O_{21}\}$ pentagonal units, four hexagonal channels, and four heptagonal channels.[38,39] Complete structural models that include site occupancy information currently only exist for the MoVNbTeO,[38,39] MoVTaTeO,[27] and MoVSbO[43] catalysts; other variants sharing the same orthorhombic framework are typically identified through XRD peak matching routines. Of these frameworks with pentagonal $\{Mo_6O_{21}\}$ building units, significant vanadium substitution appears to occur only in the M1-type, the Mo_5O_{14}-type, and the trigonal phase.

The Mo_5O_{14} phase was originally reported by Kihlborg et al. as a metastable phase that decomposes upon prolonged heating.[44] Initial single-crystal studies suggested that this phase had tetragonal symmetry; however, subtle superlattice reflections corresponding to a more complex superstructure have been reported.[1,3] Subsequent reports suggested that this phase can be stabilized through substitutional doping with transition metals (e.g., Ti, V, Nb, and Ta).[3−6,45−47] The initially proposed

(27) DeSanto, P.; Buttrey, D. J.; Grasselli, R. K.; Pyrz, W. D.; Lugmair, C. G.; Volpe, A. F.; Vogt, T.; Toby, B. H. *Top. Catal.* **2006**, *38*, 31.
(28) Pyrz, W. D.; Blom, D. A.; Shiju, N. R.; Guliants, V. V.; Vogt, T.; Buttrey, D. J. *Catal. Today* **2009**, *142*, 320.
(29) Guliants, V. V.; Bhandari, R.; Al-Saeedi, J. N.; Vasudevan, V. K.; Soman, R. S.; Guerrero-Perez, O.; Banares, M. A. *Appl. Catal., A* **2004**, *274*, 123.
(30) Guliants, V. V.; Bhandari, R.; Brongersma, H. H.; Knoester, A.; Gaffney, A. M.; Han, S. *J. Phys. Chem. B* **2005**, *109*, 10234.
(31) Sadakane, M.; Watanabe, N.; Katou, T.; Nodasaka, Y.; Ueda, W. *Angew. Chem., Int. Ed.* **2007**, *46*, 1493.
(32) Ueda, W.; Vitry, D.; Katou, T. *Catal. Today* **2005**, *99*, 43.
(33) Mestl, G. *J. Raman Spectrosc.* **2002**, *33*, 333.
(34) Zenkovets, G. A.; Kryukova, G. N.; Gavrilov, V. Y.; Tsybulya, S. V.; Anufrienko, V. A.; Larina, T. A.; Khabibulin, D. F.; Lapina, O. B.; Rodel, E.; Trunschke, A.; Ressler, T.; Schlogl, R. *Mater. Chem. Phys.* **2007**, *103*, 295.
(35) Baca, M.; Aouine, M.; Dubois, J. L.; Millet, J. M. M. *J. Catal.* **2005**, *233*, 234.
(36) Botella, P.; Dejoz, A.; López Nieto, J. M.; Concepcion, P.; Vazquez, M. I. *Appl. Catal. A* **2006**, *298*, 16.
(37) Ueda, W.; Endo, Y.; Watanabe, N. *Top. Catal.* **2006**, *38*, 261.
(38) DeSanto, P.; Buttrey, D. J.; Grasselli, R. K.; Lugmair, C. G.; Volpe, A. F.; Toby, B. H.; Vogt, T. *Z. Kristallogr.* **2004**, *219*, 152.
(39) Murayama, H.; Vitry, D.; Ueda, W.; Fuchs, G.; Anne, M.; Dubois, J. L. *App. Catal., A* **2007**, *318*, 137.
(40) Kihlborg, L. *Acta Chem. Scand.* **1960**, *14*, 1612.
(41) Magnéli, A. *Arkiv Kemi* **1949**, *1*, 223.
(42) Lundberg, M.; Sundberg, M. *Ultramicroscopy* **1993**, *52*, 429.
(43) Sadakane, M.; Yamagata, K.; Kodato, K.; Endo, K.; Toriumi, K.; Ozawa, Y.; Ozeki, T.; Nagai, T.; Matsui, Y.; Sakaguchi, N.; Pyrz, W. D.; Buttrey, D. J.; Blom, D. A.; Vogt, T.; Ueda, W. *Angew. Chem., Int. Ed.* **2009**, *48*, 3782.
(44) Kihlborg, L. *Acta Chem. Scand.* **1959**, *13*, 954.
(45) Ekstrom, T. *Acta Chem. Scand.* **1972**, *26*, 1843.
(46) Ekstrom, T.; Nygren, M. *Acta Chem. Scand.* **1972**, *26*, 1836.
(47) Ekstrom, T.; Tilley, R. J. D. *J. Solid State Chem.* **1976**, *19*, 125.

tetragonal unit cell is comprised of four $\{Mo_6O_{21}\}$ pentagonal units, eight five-member rings, two six-member rings, and two four-member rings. Yamazoe and Kihlborg later prepared small single crystals of a Ta-doped Mo_5O_{14} variant suitable for 4-circle diffraction studies and determined that the superlattice was due to doubling of the pseudotetragonal *a*-axis, resulting in orthorhombic symmetry (SG: $Pb2_1a$ (No. 29), $a = 45.75$ Å, $b = 22.87$ Å, $c = 4.0023$ Å).[3] Recent studies of Mo_5O_{14} doped with various elements, (namely V and W in the case of catalysts presently studied for partial methanol oxidation) commonly refer to the tetragonal subcell and suggest that the superlattice reflections are either absent or insufficiently resolved.[10,11,33,34] Concerning the location of the substituted atoms, recent studies by Zenkovets et al. suggest that V and W likely substitute into positions otherwise occupied by Mo, but they could not definitively assign specific sites.[34]

The trigonal phase recently discovered by Sadakane et al. has thus far only been observed in the ternary MoVO system. The trigonal phase is similar to the M1-type phase in that it contains both hexagonal and heptagonal rings. The unit cell contains two six-member rings and a cluster of three seven-member rings, which we will henceforth refer to as the heptagonal triplet.[31] Initial refinement of powder X-ray diffraction data resulted in some considerable uncertainty ($R_{wp} = 12.2\%$).[31]

In this work, we use aberration-corrected high-angle annular dark-field (HAADF) imaging to study various hydrothermally prepared MoVO phases. One advantage of transmission electron microscopy imaging as opposed to bulk diffraction techniques is the ability to analyze a single crystallite present within mixed-phase assemblages; therefore, contributions from other phases are eliminated. This was particularly important in this study because each of the analyzed samples did contain some dilute impurity phases. Analysis of the M1-type MoVO phase led to the development of a preliminary structural model that provides estimated coordinates and site occupancies. For the Mo_5O_{14}-type phase, we compare our HAADF derived model to the initial model of Yamazoe and Kihlborg.[3] In the MoVO case studied here, it was possible to distinguish V-containing sites within the structure through the analysis of image contrast; the contrast in HAADF images scales roughly with the square of the atomic number.[48,49] For the trigonal model, we were able to confirm the basic features of the proposed model of Sadakane et al.[31]

2. Experimental Methods

2.1. Catalyst Preparation. Preparation of an M1-type phase MoVO: $(NH_4)_6Mo_7O_{24}\cdot 4H_2O$ (8.82 g, 50 mmol) dissolved in water (120 mL) was mixed at 298 K with $VOSO_4\cdot nH_2O$ (3.28 g, $n = 5.4$, 12.5 mmol) dissolved in water (120 mL). The resulting solution was stirred for 10 min, then transferred to a 300 mL Teflon linear of a stainless-steel autoclave in which a folded Teflon sheet (thickness: 0.1 mm, ca. 4000 cm^2) was inserted. The pH value of the solution was ca. 3.2. The reaction mixture was purged with nitrogen for 10 min then heated at 448 K for 48 h. A gray solid (about 2.3 g) was isolated from the reaction mixture by filtration, washed with water, and dried at 353 K overnight. The solid was purified by treatment with oxalic acid: dry solid (2.0 g) was added to an aqueous solution of oxalic acid (0.4 M, 50 mL) and this mixture was stirred at 333 K for 30 min. The solid was isolated from the suspension by filtration, washed with water, and dried at 353 K overnight (1.0 g).

Formula from elemental analysis $Mo_{29}V_{11}O_{112}(NH_4)_4(H_2O)_8$. Elemental anal. Calcd wt%: Mo, 52.0; V, 10.5; O, 35.9; N, 1.0; H, 0.3. Found wt%: Mo, 51.8; V, 10.9; O, 35.8; N, 1.1; H, 0.6; total, 100.2. Complete elemental analysis was carried out by Mikroanalytisches Labor Pascher (Remagen, Germany).

Preparation of Mo_5O_{14}-type MoVO: The M1-type Mo_3VO_x (0.5 g) was placed in a conventional calcination furnace (FP 32, Yamato) and heated at 10 K min^{-1} to 673 K, and the temperature was kept at 673 K for 2 h in air. Then, the air-calcined M1-type Mo_3VO_x (0.5 g) was calcined in a tube furnace (inner diameter ca. 12 mm) under a nitrogen flow of 50 mL min^{-1}. The temperature was raised at a rate of 10 K min^{-1} to 848 K and held for 2 h.

Formula from bulk elemental analysis $Mo_{29}V_{11}O_{112}$. Elemental anal. Calcd wt%: Mo, 54.1; V, 10.9; O, 34.9; N, 0.0; H, 0.0. Found wt%: Mo, 54.2; V, 11.6; O, 34.9; N, 0.05; H, 0.05; total, 100.3.

Preparation of trigonal MoVO: $(NH_4)_6Mo_7O_{24}\cdot 4H_2O$ (8.82 g, 50 mmol) dissolved in water (120 mL) was mixed at 298 K with $VOSO_4\cdot nH_2O$ (3.28 g, $n = 5.4$, 12.5 mmol) dissolved in water (120 mL). The resulting solution was stirred for 10 min and then transferred to a 300 mL Teflon liner in a stainless-steel autoclave. The pH value of the solution was adjusted to 2.2 with dilute sulfuric acid (2 mL of concentrated sulfuric acid (min. 95%) in 20 mL of water). The reaction mixture was purged with nitrogen for 10 min then heated at 448 K for 20 h. A gray solid (about 5 g) was isolated from the reaction mixture by filtration, washed with water, and dried at 353 K overnight. The crude trigonal Mo_3VO_x was purified by treatment with oxalic acid: dry solid (4.0 g) was added to an aqueous solution of oxalic acid (0.4 M, 100 mL) and this mixture was stirred at 333 K for 30 min. The solid was isolated from the suspension by filtration, washed with water, and dried at 353 K overnight (0.8 g).

The ratio of Mo:V atoms determined by inductively coupled plasma atomic emission spectroscopy (ICP-AES) was about 3:1.[31]

2.2. Electron Microscopy. Aberration-corrected HR-STEM at 200 kV was used to image the materials with a JEOL 2100F equipped with a CEOS C_s-corrector on the illumination system at the Electron Microscopy Center of the University of South Carolina. The geometrical aberrations were measured and controlled to provide less than a $\pi/4$ phase shift of the incoming electron wave over the probe-defining aperture of 15.4 mrad. HAADF STEM images were acquired on a Fischione model 3000 HAADF detector with a camera length such that the inner cutoff angle of the detector was at least 75 mrad. The scanning acquisition was synchronized to the 60 Hz AC electrical power to minimize 60 Hz noise in the images and a pixel dwell time range between 7 and 32 μs was selected. Each sample was prepared for STEM by finely grinding the as-prepared catalyst specimen and then dipping a holey-carbon coated Cu grid into the powder. Full details for the interpretation and analysis of

(48) Howie, A. *J. Microsc.* **1979**, *117*, 11.
(49) Varela, M.; Lupini, A. R.; van Benthem, K.; Borisevich, A. Y.; Chisholm, M. F.; Shibata, N.; Abe, E.; Pennycook, S. J. *Ann. Rev. Mater. Res.* **2005**, *35*, 539.

the acquired micrographs were presented previously.[25,28,50] Selected-area electron diffraction (SAED) was completed using a JEOL 2000FX TEM operated at 200 keV using a camera length of 80 cm and an acquisition time of 90 s.

2.3. Powder XRD. Powder XRD pattern was recorded on a diffractometer (RINT Ultima+; Rigaku) with CuKα radiation (tube voltage: 40 kV, tube current: 20 mA) equipped with a graphite monochromator.

3. Results and Discussion

3.1. Ideal MoVO Models. Ideal model structures for the M1-type, Mo_5O_{14}-type, and trigonal MoVO oxides are shown in Figure 1. The model for the M1-type MoVO was idealized by modification of the refined MoVTeNbO model of DeSanto et al.[38] In this modification, Mo replaces Nb in the pentagonal biprismatic site and the Te atoms have been omitted from the hexagonal and heptagonal channels. The model for the Mo_5O_{14}-type MoVO was derived from the tetragonal subcell of Yamozoe and Kihlborg for the parent Mo_5O_{14}.[3] The trigonal model was adapted from that proposed by Sadakane et al. based on powder X-ray diffraction.[31]

The pentagonal units in each of the structural variants are interconnected in various ways by several types of $\{MO_6\}$ octahedra, where M represents Mo or V; we will refer to these octahedra that join the pentagonal units as "linking sites". The structural variations result from variations in the number and configuration of these linking sites. In the M1-type structure, three distinct classes of linking sites are observed: (1) One type (green) is corner-shared with pairs of octahedra within two different pentagonal units. (2) A second type (red) is corner-shared with two octahedra within one pentagonal unit and also to two other linking octahedra. (3) A third type (light blue) is corner-shared with four other linking octahedra.

In the Mo_5O_{14}-type structure, two different types of linking sites exist: (1) one type (red) is corner-shared with two of the octahedra within a single pentagonal unit and also to two similar linking octahedra; (2) another type (green) is corner-shared with two of the octahedra within one pentagonal unit, corner-shared with a single octahedron within a second pentagonal unit, and corner-shared with a neighboring linking site of the same type.

Finally, in the trigonal structure, two different types of linking site exist: (1) one type (green) is corner-shared with pairs of octahedra from within two different pentagonal units; (2) the second type (red) is corner-shared with two octahedra within one pentagonal unit and with two similar linking octahedra.

3.2. Powder X-ray Diffraction. Powder X-ray diffraction shown in Figure 2 was used to characterize the as-synthesized bulk product from the M1-type, Mo_5O_{14}-type, and trigonal MoVO preparations. All three samples appear to be well-crystallized because the peaks are sharp. By peak profiling against previously published results for

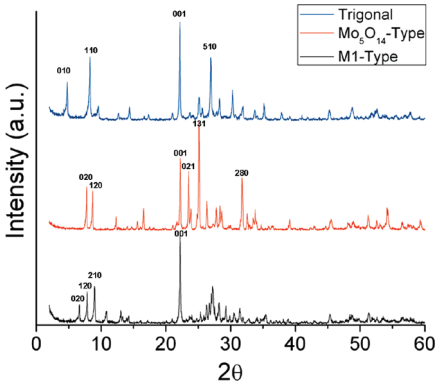

Figure 2. Powder XRD patterns of M1-type MoVO, Mo_5O_{14}-type MoVO, and trigonal MoVO.

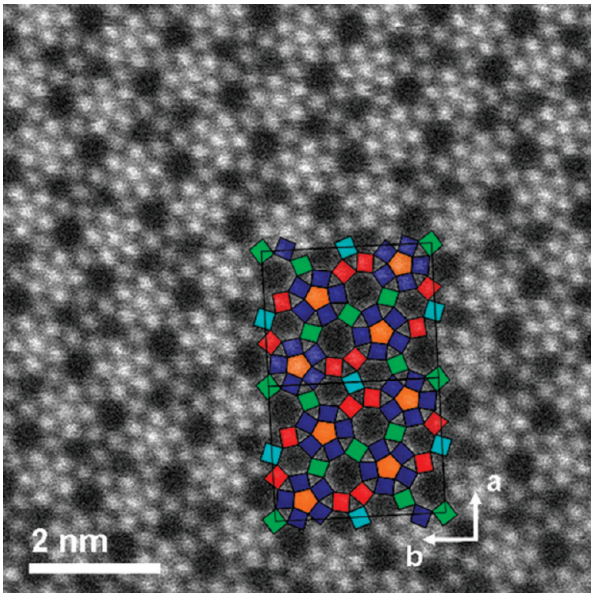

Figure 3. A raw high-resolution HAADF image of the two-component M1-type MoVO phase viewed down the [001] direction. A superimposed image of the idealized model demonstrates good qualitative agreement. Note that both the heptagonal and hexagonal channels are vacant.

the M1-type,[38] trigonal,[31] and Mo_5O_{14}-type phases,[11] the major peaks were appropriately indexed and each phase was subsequently synthesized in nearly phase pure form.

3.3. TEM Analysis of the M1-Type MoVO. A high-resolution [001] HAADF image along with a superimposed rendering of the idealized M1-type framework is shown in Figure 3. Good qualitative agreement between the idealized model and the HAADF image indicates that the atomic columns within this sample match well with the corresponding sites in the well-characterized MoVNbTeO form of the M1 phase. This result was not surprising because our previous studies have shown that the atomic positions within the M1 phase are independent of the catalyst formulation, and elemental substitutions only alter the occupancies.[28] It is clear from the image that both the hexagonal and heptagonal channels are indeed vacant, as would be expected for a formulation that excludes intercalant species (Te, Sb, etc.). Lastly, consistent with our prior results for the MoVNbTeO case,[25,28,50] the

(50) Pyrz, W. D.; Blom, D. A.; Shiju, N. R.; Guliants, V. V.; Vogt, T.; Buttrey, D. J. *J. Phys. Chem. C* **2008**, *112*, 10043.

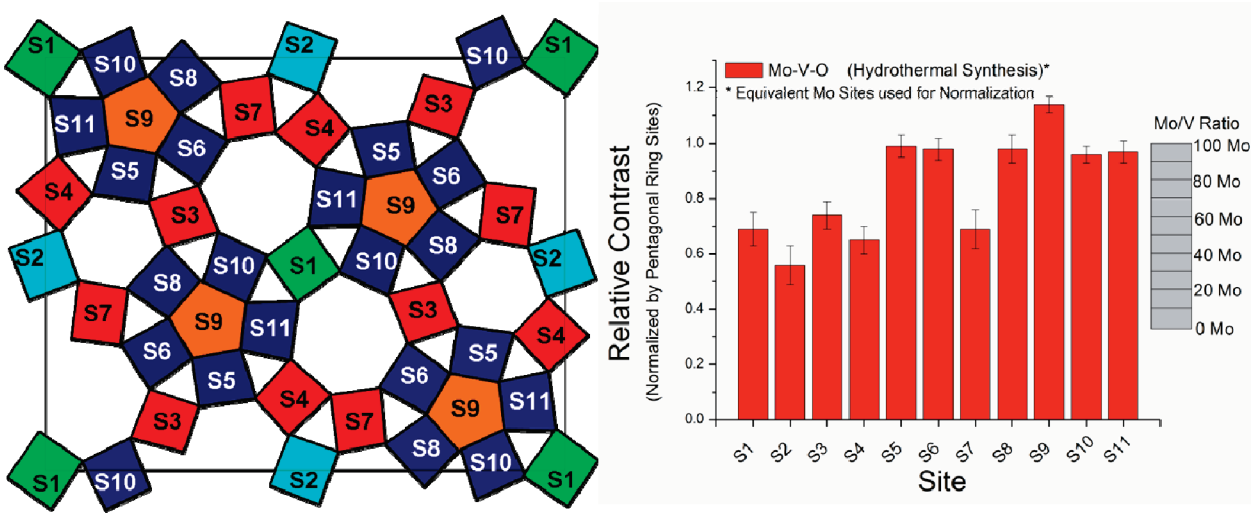

Figure 4. Idealized orthorhombic model with labeled atomic sites (left). Plot showing the relative contrast ratio for each site within the M1-type structure (right). The scale bar on the right shows the relationship between the contrast ratio and the composition of Mo or V in each atomic site assuming a Z^2 scattering relationship.

linking sites connecting the pentagonal units exhibit diminished contrast, indicating partial occupancy by V.

Using the image interpretation strategies from our previous studies,[25,28,50] specifically assuming that the image contrast scales roughly with Z^2, a contrast map was developed and is presented in Figure 4. We assume that the metal sites of the pentagonal ring are chemically similar to those containing only Mo or Nb in the MoVNbTeO case. Therefore, if we normalize all columns by the average measured intensity of the pentagonal ring metal sites, then a contrast ratio of unity indicates 100% Mo occupancy. Indeed, this initial assumption appears valid, as all the sites contained within the pentagonal rings (S5, S6, S8, S10, and S11) exhibit contrast ratios that are approximately one. However, the contrast ratio for the pentagonal biprismatic center site is about 15% higher than the surrounding sites. This elevated contrast ratio is likely due to contrast contributions from the neighboring atomic columns since the pentagonal center has the highest electron density (i.e., being higher in oxygen coordination and not adjacent to any channels formed by four-, five-, or six-member rings). However, confirmation of this assertion requires image simulation, which is planned for future studies. Analysis of the mixed occupancy sites reveals V occupancies corresponding to approximately 48, 66, 39, 52, and 48% for sites S1, S2, S3, S4, and S7, respectively. This leads to an overall stoichiometry for the formula unit of $Mo_{8.06}V_{1.94}O_{28}$ (equivalent to $Mo_{1.00}V_{0.24}O_x$ in previous reports[31]). Energy-dispersive X-ray spectroscopy (EDS) measurements on two of the analyzed crystallites yielded an average formula unit of $Mo_{7.01}V_{2.99}O_{28}$. These results are in reasonable agreement with the Mo:V composition obtained by bulk elemental analysis, which would correspond to an expected formula unit of $Mo_{7.25}V_{2.75}O_{28}$. The discrepancy observed for HAADF image quantification is likely due to uncertainties associated with assumptions used. As mentioned, the image simulation experiments are crucial for increasing confidence in the quantitative results based on the image interpretation assumptions and to explore the sensitivity of the observed contrast with sample thickness or small angular deviations from perfect [001] zone orientation.

The results from the HAADF studies have provided estimates for many of the adjustable parameters required for future Rietveld refinements. For the M1-type MoVO phase, initial coordinates for the atomic positions should be taken from the prior MoVNbTeO refinements[38,39] and the fractional occupancies from these high-resolution HAADF studies should be used.

3.4. TEM Analysis of Mo_5O_{14}-Type MoVO. Powder XRD analyses indicate that secondary heat treatment of the M1-type phase can be used to transform the structure to a V-substituted Mo_5O_{14}-type variant (Figure 2). However, the conversion was not complete, since the M1-type and Mo_5O_{14}-type phases were always found to coexist by TEM analysis. A high-resolution HAADF micrograph of the Mo_5O_{14}-type phase observed down the [00$\bar{1}$] direction is presented in Figure 5a. The same image was smoothed using a Gaussian filter as shown in Figure 5b. A section from both the raw and smoothed image was magnified and is shown in images c and d in Figure 5. A superimposed rendering of the ideal subcell model was added to the magnified portion of the smoothed image in Figure 5d. Comparison of the HAADF image with the idealized model indicates good qualitative agreement. Direct measurements of the *x, y* coordinates from the HAADF images match well with the model coordinates from the tetragonal subcell proposed by Yamozoe and Kihlborg.[3] The average deviation between the model coordinates and the HAADF measurements was ~0.10 Å. However, it is still unclear as to whether this MoVO sample exhibits the subtle orthorhombic distortion in the revised model proposed by Yamozoe and Kihlborg,[3] or if it has the undistorted tetragonal symmetry as shown in Figure 1. Inspection of [001] SAED patterns a and b in Figure 6 leads us to conclude that the symmetry is tetragonal in that superlattice reflections consistent with a doubling

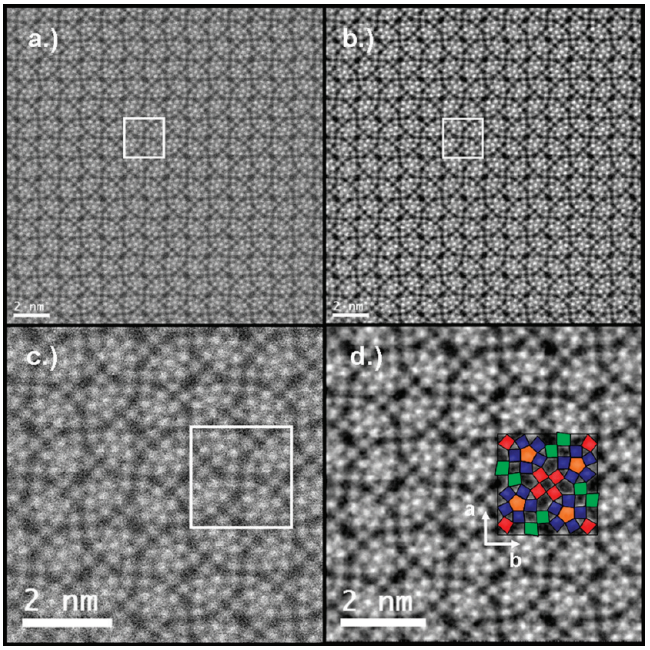

Figure 5. (a) Raw HAADF image of the Mo_5O_{14}-type MoVO phase viewed down the [00$\bar{1}$] direction. (b) Same image after the application of a Gaussian filter for noise reduction (c) Magnification of the raw image. (d) Magnification of the filtered image with the Mo_5O_{14}-type model superimposed on top.

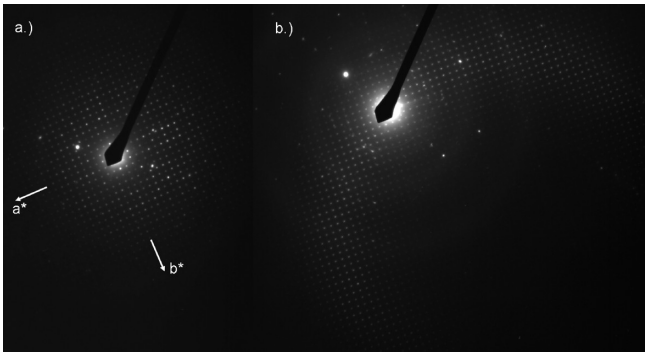

Figure 6. (a) $s = 0$ SAED pattern of the [001] zone axis from the MoVO Mo_5O_{14}-type phase. The lattice parameters are $a \approx b \approx 22.9$ Å. (b) SAED pattern tilted away from $s = 0$ to reveal higher-order reflections. Close inspection suggests that the V-substituted form of Mo_5O_{14} may have tetragonal symmetry because there is no evidence of superlattice reflections along a^* or b^* and the absence conditions along a^* and b^* for the $Pb2_1a$ space group (No. 29) are not present. Note that the extra reflections that do not appear part of the square pattern are from adjacent crystallites that contribute to the observed diffraction patterns.

of either the a or b parameter are not evident. A lattice spacing of ~23 Å was measured for the principle basal plane directions. These distances are consistent with the basal lattice constant previously reported for the tetragonal subcell.[3] Furthermore, the proposed orthorhombic space group $Pb2_1a$ (No. 29)[3] should exhibit an absence condition along a^* and b^* that is not observed in the patterns displayed in patterns a and b in Figure 6. Analysis of the [100] or [010] zones would be required to determine the appropriate space group for the Mo_5O_{14}-type phase synthesized in this study. The incomplete transformation of the M1-type phase to the Mo_5O_{14}-type phase significantly hinders this experiment. Differentiation of the Mo_5O_{14}-type phase from the M1-type impurity using the [100] or [010] zones is problematic since the c-axis for both phases are nearly identical. Initial verification of a crystallite with the Mo_5O_{14}-type phase using the [001] zone is not possible because the tilting capabilities of the TEM holder do not allow the analysis of zones that are orthogonal to one another. From these diffraction results, we can speculate that the symmetry is tetragonal, but additional studies with a phase-pure sample are necessary and are currently being planned.

Qualitative comparison of the atomic-column intensity between the pentagonal ring sites (S4−S9) and the linking sites (S1−S3, S10) from the raw HAADF image in Figure 7 indicates compositional differences due to contrast variations. Using the same image interpretation strategies from the previous section, a contrast map was developed (Figure 7c). The significant variability in the measured contrast ratios confirms the qualitative observation suggesting compositional differences between the sites in the pentagonal units and the linkers. The measurements suggest that the V is located in these linking sites with occupancies between 45 and 60% leading to an estimated stoichiometry of $Mo_{4.10}V_{0.90}O_{14}$. EDS analysis of two crystallites led to an average formula unit of $Mo_{3.66}V_{1.34}O_{14}$. Both results are similar to the Mo/V composition obtained by bulk elemental analysis, which would be expected to give $Mo_{3.62}V_{1.38}O_{14}$. The approximate nature of the assumptions used for HAADF analysis are the likely cause for the discrepancy between the HAADF image interpretation results and the expected composition based on the EDS results and the nominal synthesis Mo/V ratio. The HAADF evidence for V in the linking sites is consistent with inferences by Schlögl et al.[34] from precursor solution studies associated with synthesis of Mo_5O_{14}-type MoVWO materials. Furthermore, this result is also consistent with the occupancy of V within similar linking sites in the MoVTeNbO and MoVTeTaO structures.[25,28,50]

3.5. TEM Analysis of Trigonal MoVO. The synthesis targeting the trigonal phase led to a mixed-phase powder containing the desired trigonal product in coexistence with a defective M1-type phase and crystallites in which the trigonal and M1-type phases are intergrown. An example of a well-ordered intergrown crystallite is shown in Figures 8a and an example of a defective crystallite is shown in Figure 8b. The intergrowth crystallite contains multiple trigonal and M1-type domains with typical dimensions of several square nanometers in basal projection. The defective orthorhombic crystallites exhibited only short-range order and were full of voids and trigonal-like defects. Full structural characterization of the coherently intergrown phases is the subject of a separate report.

A high-resolution HAADF image of the MoVO trigonal phase is shown in Figure 9 along with a superimposed rendering of the idealized unit cell. Comparison of the image in Figure 9 with the superimposed ideal model provides reasonable qualitative agreement. The agreement was confirmed by directly measuring x, y coordinates from the HAADF images and comparing them to the x, y coordinates from the refinement of powder X-ray

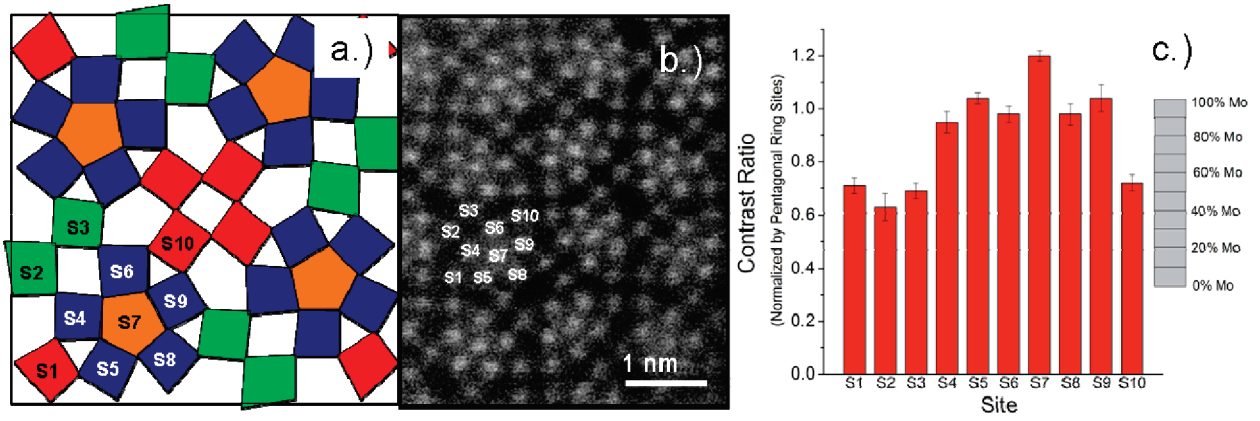

Figure 7. (a) Rendering of the Mo_5O_{14}-type model with site labels added to the lower-left quadrant. (b) HAADF micrograph showing the same lower-left quadrant of the unit cell. (c) Contrast analysis of individual atomic columns along with Mo/V composition estimates for each site based on the Z^2 Rutherford scattering assumption.

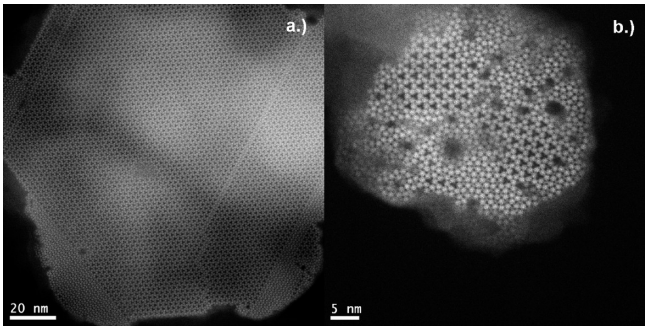

Figure 8. HAADF images showing two examples of phase intergrowth between the trigonal phase and the M1-type phase. The trigonal phase domains are easily identified by locating the triangular features that represent the heptagonal triplet.

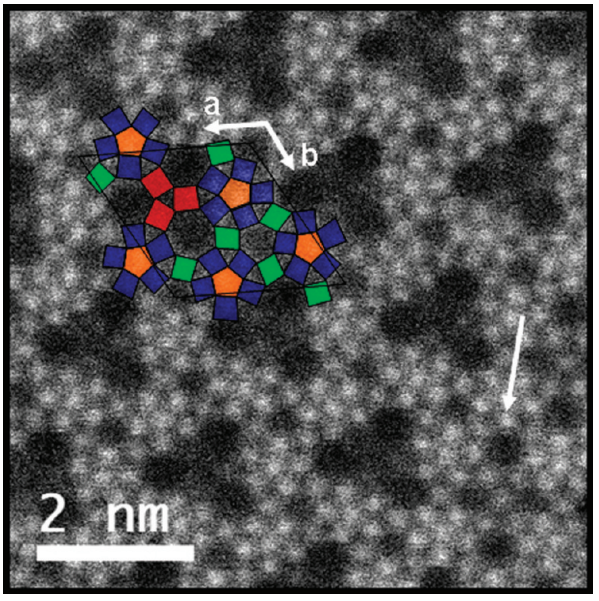

Figure 9. HAADF image of the trigonal structure observed down the [001] direction along with a superimposed idealized trigonal unit cell. The arrow points to the edge of a phase boundary between the trigonal phase and the orthorhombic phase.

diffraction data.[31] The average deviation between the HAADF coordinates and the refined coordinates was ~0.13 Å. The arrow in Figure 9 indicates the boundary between the trigonal phase and the intergrown M1-type phase.

In the HAADF image in Figure 9, the hexagonal rings are composed of well-resolved atomic columns that alternate between linking sites and pentagonal ring sites. The linking sites have contrasts that are diminished compared to those in the pentagonal units, again suggesting preferred occupancy of vanadium in the linking sites. Each seven-member ring observed in the HAADF image reveals a sequence of five well-resolved atomic columns and two poorly resolved columns. We believe that the blurring/diminished contrast in these poorly resolved sites is due to disorder along the *c*-axis; however, high V content may also contribute to the weak contrast. HAADF images in Figure 10 show several heptagonal triplets before and after Gaussian filtering. Examination of the low-contrast columns in the filtered images reveals an elongation or distortion from the usual rounded profile typical of well-resolved atomic columns. In some cases, indicated by white arrows in images b and d in Figure 10, there is evidence of some additional atomic sites within the heptagonal triplet that were not expected from the model proposed by Sadakane et al.[31] This result suggests that atoms in these columns may be staggered in a zigzag fashion along the unique *c*-axis, rather than concentrically stacked in projection. We believe that adjacent features within the trigonal holes are zigzagged since there appears to be too little space available for these to be coplanar in *z*. However, special care must be taken when trying to interpret processed images to avoid artifacts. For example, some of the hexagonal channels in Figure 10c appear empty before smoothing, but occupied afterward (Figure 10d); therefore, additional evidence will be required to confirm or refute the additional occupancy within the heptagonal triplet. Unfortunately, effective quantitative analysis of the vanadium occupancies was not possible because of these regions of disorder as well as thickness variations caused by multiple particles overlapping with one another. Attempts to find nonoverlapping crystallites have been unsuccessful so far because of the difficulty in finding well-formed [001] particles (the typical morphology of these materials is

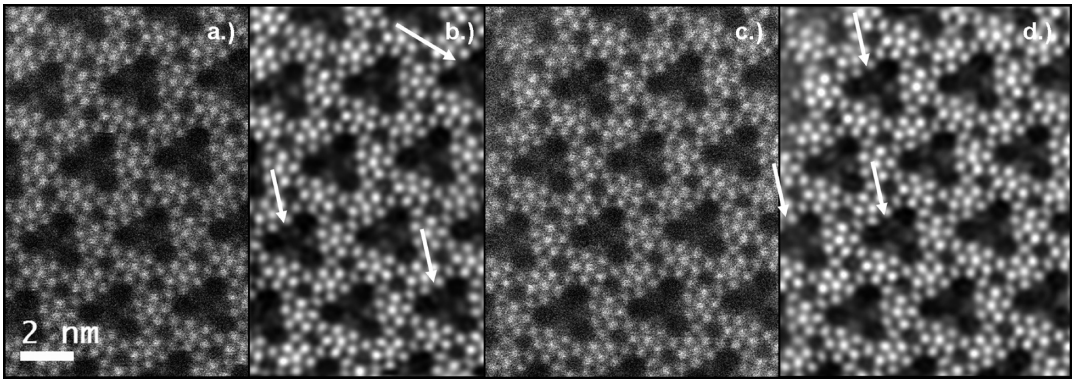

Figure 10. (a) Raw high-resolution HAADF image down the [001] direction of the trigonal MoVO phase. (b) Image in part a following the application of a Gaussian filter. (c) Raw HAADF image from a different region of the crystallite. (d) Image in part c following the application of a Gaussian filter. The scale bar in part a applies to all images and the arrows point toward heptagonal triplets that appear to have additional atomic columns that were not expected on the basis of the proposed trigonal model by Sadakane et al.[31]

needle-like with the *c*-axis as the long dimension, thus limiting the number of crystallites in a favorable orientation).

4. Conclusions

HAADF STEM imaging was used to study various MoVO phases. For the M1-type phase, HAADF image analysis confirmed that the atomic positions remain fixed and independent of whether the M1 phases contains only Mo and V or is doped with Ta, Te, or Nb. Contrast analysis suggested mixed Mo and V occupancy in the octahedral sites linking the pentagonal units as well as providing estimates for the Mo/V ratios. Combining both results will lead to a significantly improved starting model for a full Rietveld analysis. The occupancies in the M1 phase are of significant interest to many in the catalysis community because the proficiency for propane (amm)-oxidation may be associated with the distribution of vanadium in the linking sites on the (001) surface. Although we find roughly 2 nm of amorphous material covering surfaces belonging to the [001] zone, the existence or absence of an amorphous overlayer on the (001) face remains under debate.

Direct image interpretation for the V-substituted Mo_5O_{14} phase provided evidence of V occupation primarily in the $\{MoO_6\}$ linking octahedra that interconnect the pentagonal $\{Mo_6O_{21}\}$ units. SAED studies suggest that the structure of the Mo_5O_{14} analog is likely to be tetragonal rather than the orthorhombically-distorted variant reported by Yamazoe and Kihlborg.[3] HAADF-derived atomic coordinates were consistent with the metal positions of the tetragonal subcell proposed by Yamazoe and Kihlborg.[3]

HAADF analysis of the trigonal phase provides reasonable support for the model proposed by Sadakane et al.[31] apart from the remaining issues concerning the disordered sites within the heptagonal triplet. Gaussian filtering of high-resolution images provides strong support for the proposed nature of the atomic disorder in these sites. The filtered images suggest a possible zigzag pattern along the *c*-axis for heptagonal triplet channel occupancies. The enhanced spatial resolution and chemical sensitivity of aberration-corrected HAADF imaging has provided new insights toward understanding the phase equilibrium of complex MoVO oxide materials. It has also provided a method for the detection of dilute impurity phases that otherwise would have been overlooked using standard bulk characterization techniques. The careful analysis of the MoVO systems using aberration-corrected imaging has led to the discovery of various defects and phase intergrowths.

Acknowledgment. W.D.P. and D.J.B. acknowledge Dr. Chaoying Ni, Frank Kriss, and the W. M. Keck Electron Microscopy Facility for access and assistance in the electron diffraction studies. M.S. and W.U. thank Grants-in-Aid for Scientific Research (Scientific Research "A") of the Ministry of Education, Culture, Sports, Science, Japan, for financial support. D.A.B. and T.V. would like to thank the State of South Carolina for direct support of the NanoCenter at the University of South Carolina.